lubricants

MDPI

Article

Wear Development in Oscillating Rolling Element Bearings

Sebastian Wandel [1,*], Arne Bartschat [2], Jakob Glodowski [1], Norbert Bader [3] and Gerhard Poll [1]

[1] Institute of Machine Design and Tribology (IMKT), Leibniz Universität Hannover, 30823 Garbsen, Germany
[2] Fraunhofer Institute for Wind Energy Systems IWES, Am Schleusengraben 22, 21029 Hamburg, Germany
[3] Faculty of Engineering Technology, University of Twente, 7500 AE Enschede, The Netherlands
* Correspondence: wandel@imkt.uni-hannover.de

Abstract: Rotor blade bearings enable rotor blades to pivot about their longitudinal axis and thus control the power output and reduce the loads acting on the wind turbine. Over a design period of 20 years, rolling bearings are exposed to frequent oscillation movements with amplitude ratios of $x/2b > 1$, especially due to new control concepts such as Individual Pitch Control, which can lead to wear and a reduction in service life. The objective of this paper was to identify the dominant wear mechanisms and their consequences for the operation of oscillating bearings. Oscillating experiments with an increasing number of cycles on the angular contact ball bearings of two different sizes (types 7208 and 7220) show that the damage initiation starts with adhesive and corrosive wear mechanisms, which result in a sharp increase in the torque as well as the wear volume on the bearing raceway. As the number of cycles increases, an abrasive mechanism occurs, resulting in a lower slope of the wear curve and a smoothing of the resulting wear depressions. The wear and torque curves were evaluated and classified using an energy-wear approach according to FOUVRY.

Keywords: grease lubrication; false brinelling; oscillating bearing; pitch bearing; wear

Citation: Wandel, S.; Bartschat, A.; Glodowski, J.; Bader, N.; Poll, G. Wear Development in Oscillating Rolling Element Bearings. *Lubricants* **2023**, *11*, 117. https://doi.org/10.3390/lubricants11030117

Received: 24 January 2023
Revised: 15 February 2023
Accepted: 18 February 2023
Published: 7 March 2023

1. Introduction

1.1. Oscillating Bearings in Wind Turbines

Grease-lubricated oscillating rolling element bearings can be found in various industrial applications. One example is that of the rotor blade bearings of wind turbines. Rotor blade bearings are large slewing bearings. Stochastic wind conditions lead to transient loads acting on the bearings in 5 degrees of freedom. In addition, interface parts such as rotor blades and the hub can have complex and changing stiffness properties, which affect the load distribution and deformation of the bearings. Furthermore, the environmental characteristics, such as low temperatures and high humidity, add to the challenging operating conditions.

Several bearing designs are in use, with the four-point contact double-row ball bearing being the most common design for modern wind turbines. The blade bearing connects the rotor blade to the hub and enables the rotation of the blade along its longitudinal axis. This so-called pitching movement changes the angle of attack of the rotor blades and thus influences the power output and the loads acting on the wind turbine. The pitch controller changes the pitch angle of all rotor blades to limit the power output above the rated wind speed and keeps the rotational speed of the rotor constant. This is usually called a collective pitch control (CPC), as all three blades are subject to the same pitch angle changes [1]. In addition, there are more advanced pitch control strategies which enable other features such as load mitigation or wake steering [2,3]. It is common among more advanced pitch controller set ups that every blade is controlled individually. Hence, the controller can react to different inflow conditions across the rotor plane—such as those induced by the vertical wind shear—with each individual blade to lower the fatigue relevant load cycles on the structure of the wind turbine. This method is usually called individual pitch control (IPC). Recent investigations have shown that, in contrast to CPC, IPC can decrease the number of

very small oscillation movements and lead to generally larger oscillation amplitudes [4,5]. These oscillation angles depend on the individual controller and turbine design and do not allow for a general statement. However, it can be stated, with respect to the available work based on the reference wind turbine models, that the amount of oscillating movement with an amplitude ratio $x/2b > 2$ is higher when using an IPC controller. The amplitude ratio is defined as the quotient of the distance that the center of the contact travels relative to the bearing raceway x and the width of the contact ellipse $2b$. Figure 1 illustrates the amplitude ratio $x/2b$.

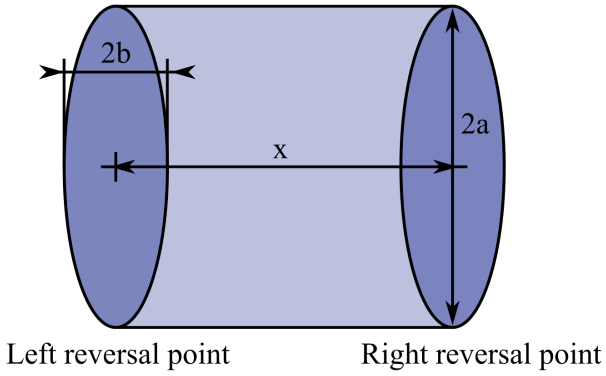

Figure 1. Illustration of the amplitude ratio $x/2b$. In dark blue, the Hertzian contact ellipse in the reversal points of the oscillatory motion is shown.

In addition, BEHNKE ET AL. and WANDEL ET AL. found that very small oscillation movements are most likely not the most critical ones when in terms of wear as a failure mode and the middle range of amplitude ratios has a greater impact [5,6] . However, the stochastic nature of the wind and operating conditions of the wind turbine as well as the influence of the specific order of occurrence of cyclic movements of the blade bearings makes rating the risk of wear damage a very difficult topic. Thus, there is a certain risk that site-specific wind conditions stay between cut in and rated wind speeds for long periods of time and IPC operation can add up over 13,000 cycles without a significant change in the mean oscillation angle [7]. This makes a better understanding of the wear mechanisms, especially for a comparably low number of valuable oscillation cycles. This paper focuses on analyzing those small angular oscillations with constant oscillation frequency and amplitude regarding their impact on wear development. The next chapter will describe these wear-provoking operating conditions in more detail.

1.2. Wear in Oscillating Bearings

The wear problem in oscillating rolling bearings has been known since 1937, when ALMEN investigated the damage caused to the wheel bearings of passenger cars transported on diesel ships and introduced the name *False Brinelling* for such wear marks [8]. It has been understood through the works of, e.g., VINGSBO and GREBE, that the amplitude ratio $x/2b$ and thus the oscillation angle hold decisive influence over the underlying wear mechanisms [9,10]. Bearings subjected to oscillations with very small amplitudes $x/2b < 1$ can result in surface-induced fatigue cracks. Detailed studies on these operating conditions have been carried out by GREBE, SCHWACK, SHADOW, and others [11–13]. To date, it has been assumed that small oscillation angles are more critical with regard to wear initiation, and that increasing amplitude ratios lead to improved lubricant film formation preventing wear. However, investigations by WANDEL have shown that an amplitude ratio of $x/2b = 4$, for example, can be more critical than an amplitude ratio of $x/2b = 1$ [6]. Only significantly larger amplitude ratios counteract the initiation of wear. As stated before, new controller concepts such as IPC increasingly cause oscillations with amplitude ratios $x/2b > 1$. In this amplitude range, the number of research papers focusing on wear is

significantly lower than in the range of $x/2b < 1$. In 1997, PHANER-GROUTORBE used scanning tunnel microscopy (STM) to show how the microscopic surface structure locally changes in individual wear marks on the bearing raceway surface. Other publications have dealt with lubrication mechanisms and the effectiveness of greases in preventing wear damage. Summarized from the publications of MARUYAMA, SAATCHI, WANDEL, KITA, and SHIMA, a high oil release as well as a low grease consistency and a high mobility of the base oil are crucial to prevent wear [14–18]. The suitability of lubricants for oscillating bearing applications is often determined using standard tests such as the Fafnir test and the SNR-FEB2-test [19,20]. The Fafnir test is specified in an ASTM standard, and uses thrust ball bearings with an outside diameter of 35.69 mm oscillated at an amplitude ratio of $x/2b = 5.5$ and an oscillation frequency of $f = 30$ Hz for 22 hours at a maximum contact pressure in the range of $p_{max} = 1.87 - 2.28$ GPa. The European equivalent, the SNR-FEB2-test, uses type 51206 thrust ball bearings with an outer diameter of $d_o = 52$ mm that are oscillated at an amplitude ratio of $x/2b = 3.4$ and a frequency of $f = 25$ Hz for 50 h at a maximum contact pressure of $p_{max} = 2.3$ GPa. In both tests, the bearing washers are weighed before and after the test to determine the mass loss. The standard does not include the in situ measurement of the wear progress or the bearing torque, which is why the development of wear volume over time has not yet been publicly documented. The aim of this paper was to analyze the development of wear in the angular contact ball bearings that are subjected to oscillations at amplitude ratios of $2 < x/2b < 4$ which are especially interesting for IPC-controllers in wind turbines.

The loads were selected so that there is a maxmium contact pressure of 2 or 2.5 GPa. Pressures in this order of magnitude are commonly used both in wear tests in rotor blade bearings ([11,12,21]) and in the standards (SNR-FEB2, Fafnir [19,20]). In real applications, however, these pressures are subject to stochastic fluctuations.

For this purpose, each wear mark of the bearing is phenomenologically and quantitatively analyzed at different stages in the the wear progress in order to understand which wear mechanisms are active at which point in time. Thus, it can be deduced at which stage the use of protective measures such as protection runs, as reported by STAMMLER, could be effective [22]. Furthermore, a connection of the measured results to a well-known energy wear approach according to FOUVRY will be established and discussed [23]. This allows a distinction of the wear mechanisms.

2. Materials and Methods

2.1. Experimental Setup

The experiments presented in this paper were carried out on two different setups. One setup was used to perform the experiments on type 7208 angular contact ball bearings (ACBBs), whislt the other one uses type 7220 ACBB. Both types of bearings were manufactured by FAG Kugelfischer, a company based in Nürnberg, Germany. Table 1 contains the characteristics for the bearing types used. The basic structure of the test rigs is similar, and thus only one rig is explained in detail. Figure 2 shows the aforementioned test setup for the type 7208 angular contact ball bearings. A position-controlled asynchronous servo motor allows oscillation with variable amplitude and frequency. This drives a shaft on which two unsealed angular contact ball bearings are mounted in x-arrangement (face-to-face). The drive and shaft are connected by a torque measurement shaft with an integrated incremental encoder. The bearings are axially loaded by a hydraulic load unit. The temperature on the bearing outer rings during the tests is monitored by PT100 sensors of the company Fühlersysteme eNet international GmbH based in Nürnberg, Germany.

Table 1. Bearing parameters for the type 7208 and type 7220 bearings used.

Parameter	7208	7220	Unit
Type	Angular Contact Ball Bearing (ACBB)	ACBB	-
Inner Diameter d	40	100	mm
Outer Diameter D	80	180	mm
Diameter Rolling Element D_{re}	11.9	25.4	mm
Number of Rolling Elements Z	14	15	-
Contact Angle α	40	40	°
Basic Dynamic Load Rating C_1	36,000	142,000	N

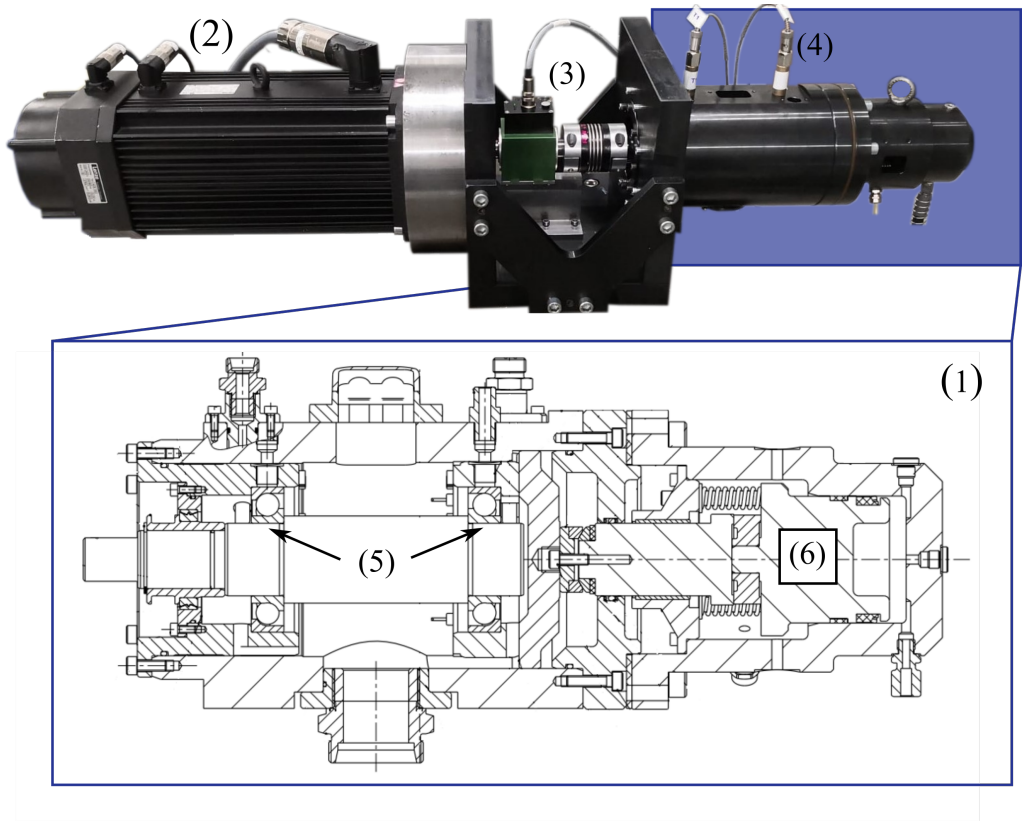

Figure 2. The upper part shows a picture of the complete test setup including the servo motor (2) of the torque shaft (3) and the test unit (4). The lower part (1) shows a drawing of the test unit that contains the two angular contact ball bearings of type 7208 (5) and the load application system (6).

2.2. Methods of Analysis

In order to gain an understanding of the mechanisms involved in the wear progression, the angle synchronous torque during the test run was recorded. Figure 3 shows two exemplary torque curves over the oscillation angle. The curve shows a torque curve of an undamaged bearing, as was first explained by DAHL ET AL. and later further discussed by TODD ET AL. [24,25]. The slope s of the curve after the reversal point comes from an elastic response of the contacting partners. At fully developed rolling the steady-state torque T_s is reached.. For an undamaged bearing, the steady-state torque is close to the maximum torque during an oscillation cycle $T_s \approxeq T_{max}$. During the course of our tests, the shape of the torque curve changes so that curves such as the blue one in Figure 3 emerge. Here, a significantly increased T_{max} is observed in the reversal points. The angle-synchronous torque allows the calculation of the dissipated friction energy E_d, which can be viewed as the integral of the enclosed areas E_{di} of N friction curves. In Figure 3, the areas E_{di} (green) and $E_{d(i+x)}$ (blue) are displayed for the exemplary torque curves.

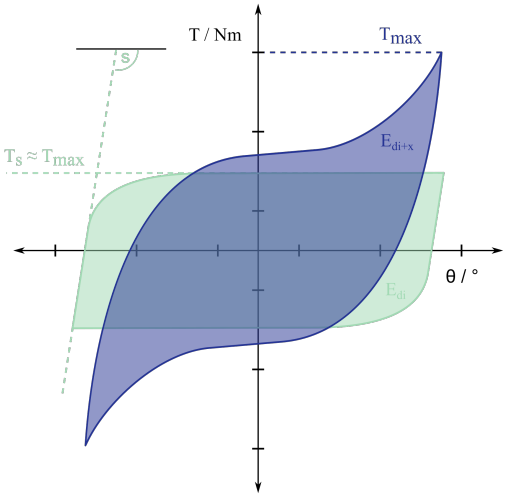

Figure 3. Two exemplary torque curves that can qualitatively arise during the experiments. In green, the torque curve of the undamaged bearing, which corresponds to the model curve set up according to DAHL with the slope s and the steady-state torque T_s, is shown. The qualitative torque at an advanced damage formation is shown in blue. The area of the curves E_{di} (green) and $E_{d(i+x)}$ (blue), shown in transparent colors, correspond to the dissipated energy for the respective oscillation cycle.

$$E_d = \sum_{i=1}^{N} E_{d,i} \tag{1}$$

The aim of the determination of the friction energy is to find a relation between the dissipated energy and wear volume on the bearing raceway according to FOUVRY [23].

A laser scanning microscope is used to determine the worn material volume on the bearing raceway surface. To calculate the wear volume of the 7208 bearings, a topographical image of the whole wear mark with the surrounding non-worn areas is acquired. The non-worn areas are interpolated with second-degree functions to create a model of the original raceway surface. By subtracting the worn surface from the original surface, a difference image is created from which the worn volume of a damage mark is determined, as can be seen in Figure 4.

In contrast to the laser scanning microscopic measurements of the 7208 bearings, the procedure is applied differently for the larger bearings of type 7220. Due to the larger dimension of the wear mark, approximately 4 × 8 mm, the curvature of the raceway makes a complete topographic examination difficult and time consuming. Therefore, only a section of the wear mark was investigated with the laser scanning microscope using the same procedure as described above. To gain repeatable results, the lateral extension of the wear mark is investigated to find the position of the upper third part of the wear mark, which is usually characterized by the most prominent wear damage. Hence, the measured wear volume calculated for the 7220 bearing does not reflect the total amount of worn material per damage mark.Instead, it is used as a benchmark to characterize the wear damage produced by different test configurations and parameter sets. As the wear volume only covers a fraction of the wear mark, it is multiplied by factor of 15, which is derived from dividing the height of the contact ellipse at a pressure of 2.5 GPa by the height of the laser scan. The idea of this factor is to achieve a wear volume, which is closer to representing a complete wear mark. Even if the absolute values after adjusting are inaccurate, it simplifies the comparison of results.

In addition to the topography images taken with the laser scanning microscope, the optical microscopic images of the damage were taken to provide a visual assessment of the damage. However, it is not only difficult to perform laser scans for evaluating the wear volume but also difficult to process light microscopic images. The curvature

of the raceways and the shiny appearance lead to strong reflections which are difficult to avoid and interfere with the visual impression of the wear marks. Hence, the light microscopic images of the 7220 bearing raceways just show sections which cover a window of approximately 0.53 mm in height and 4.4 mm in width. Due to the different microscope used for the light microscopic images, these have far less reflections and appear more dull in comparison with the images taken from the 7208 bearings.

To compare the results of the different bearing sizes investigated in this paper with respect to the energy wear factor, the measured wear volume and measured friction torque are adjusted to describe the wear factor for a single ball raceway contact. Hence, the friction torque measured for a set of two bearings is divided by 2 and the number of ball raceway contacts per bearing.

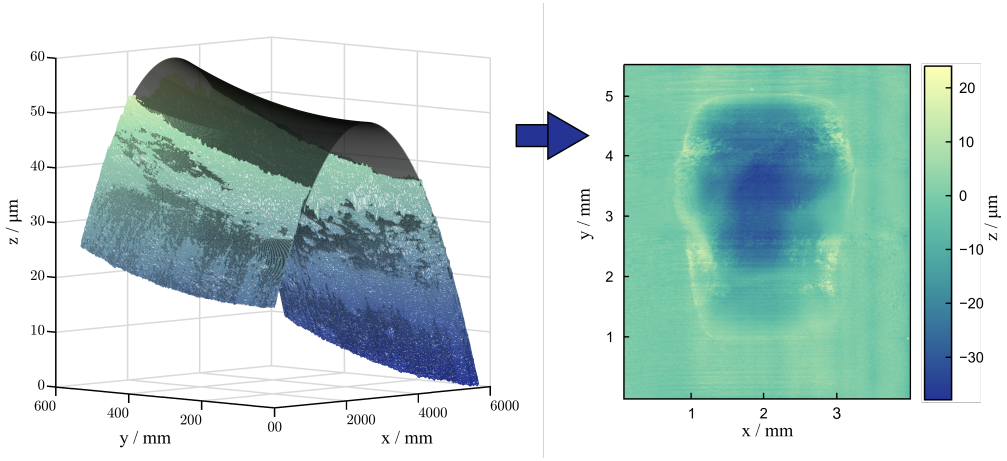

Figure 4. The left figure shows the real measured profile of a damaged raceway surface of a 7220 bearing in blue/green. The interpolated undamaged raceway surface is shown in black. The right figure shows an image of the difference of a damage mark in a 7208 bearing, which results from the difference in the interpolated surface and real profile.

2.3. Experimental Conditions

In this section, the conditions for the tests carried out on the different bearing sizes are explained in detail. All experiments were performed with a fully formulated grease paste that is commonly used in rotor blade bearing applications. The grease parameters are listed in Table 2.

Table 2. Grease properties.

Parameter	Grease 1	Unit
Thickener Type	Lithium	-
Base Oil Type	Synthetic (PAO)	-
Base Oil Viscosity	50	cSt at 40 °C
Oil Separation Rate (IP 121)	4	%
Dropping Point	>180	°C
Additives	Fully Additivated + Solid Lubricants	-

2.3.1. Experimental Condition—7208 Bearings

For this test, an axial load of 12 kN, which leads to a contact pressure $p_{H,IR}$ of 2 GPa in the contact between the inner ring and rolling element, was applied. An oscillation frequency of 5 Hz and an oscillation angle of 7° or an amplitude ratio $x/2b = 4$ were chosen.

The choice of operating conditions was based on the previously described frequent $x/2b$ ratios occurring in IPC-controllers, as well as on previously performed parameter studies with the same bearing type [6,18]. These have already shown that the conditions are particularly critical for early wear initiation. The bearings are each filled with 10 mL

of grease through a syringe. The bearings are then mounted and continuously rotated at 10 rpm for 20 rotations so that an even distribution of grease is ensured. Subsequently, the oscillating test sequence is initiated. To be able to follow the progression of the raceway damage, tests with an increasing number of cycles were conducted, i.e., a pair of bearings was run for a defined number of, e.g., 1000 cycles—subsequently dismounted, cleaned, and prepared for the optical analysis. a fresh pair of bearings was then tested for 10,000 cycles under the same test conditions and so on. The tested parameters are listed in Table 3.

Table 3. Test parameters for wear development on type 7208 and type 7220 bearings.

Parameter	7208	7220	Unit
Axial Load	12.4	90	kN
Contact Pressure	2	2.5	GPa
C_1/P_1-Ratio	5	2.8	-
Oscillation Frequency f	5	0.5	Hz
Oscillation Angle θ	7	4	°
Amplitude Ratio x/2b	4	2.6	-
Cycles	1, 5, 10, 20, 40, 80, 160	0.5, 1, 2, 3, 4, 5, 20, 40, 340, 1000	$\times 10^3$

2.3.2. Experimental Conditions on 7220 Bearings

The tests with the bearings of type 7220 are conducted at an axial load of 90 kN. This axial force translates into a contact pressure of approximately $p_{H,IR}$ of 2.5 GPa at the contacts between rolling elements and inner ring. The oscillation frequency is set to 0.5 Hz and the oscillation angle for the sinusoidal movement is 4°. This set of parameters translates to an $x/2b$ ratio of 2.6 with a frequency which is typical for the corresponding operating conditions in a wind turbine. Each of the bearings is thoroughly cleaned from corrosion protection and lubricated with approximately 160 mL of the test grease (see Table 2). After the assembly of the bearings in the test rig and before any cyclic movements are applied, the load is applied to the bearings while at least 100 full rotations are performed while checking the driving torque signal. This procedure not only ensures a proper seating of the bearings but also a good grease distribution. As with the bearings of type 7208, several tests were carried out, whereas the more general test parameters including the load, oscillating frequency, and angle were kept constant as the number of cycles was changed for different tests. The parameters are listed in Table 3.

3. Results

In this section, the light microscope images as well as the topography measurements with the laser scanning microscope are evaluated. In addition, the recorded torque is analyzed and a connection is made between the dissipated energy and the measured wear volume.

3.1. Wear Development 7208

To show how the damage marks on the inner raceway of the bearings are developing, Figure 5 shows the representative damage marks after different cycle counts. Figure 5a shows a contact area with corrosive wear starting after 1000 cycles (2). At this cycle count, most contact areas are not showing signs of severe wear, whilst others such as the one in the figure are partly showing corrosive wear. It should be noted at this point that no elemental analysis was performed to prove that these are indeed corrosion products. However, it has long been known from the literature that the reddish brown and black discolorations in the oscillating steel–steel contact are corrosion products such as hematite and magnetite [26–28]. After 20,000 cycles (Figure 5b), every contact area shows severe damage that has spread over the entire area swept by the rolling elements. In the damage mark, smaller micropitts (3) and, as a result, a rough-looking surface can be observed. In addition, reddish-brown and blackish-brown corrosive products are visible. At a more advanced stage, after 80,000 cycles, the damage pattern shown in Figure 5c appears. Some

parts of the wear mark still appear reddish-brown and on the left side at middle height a bigger material spall can be observed (5). It is also noticeable that large parts of the damage mark have been smoothed and have a mirror-like appearance (4). After 160,000 cycles (Figure 5d), as after 80,000 cycles, a material spall is found on the right side of the mark at mid-height. Almost no corrosive products can be seen in the damage mark; these are only found in the outline of the mark. At this point, the entire ground of the damage mark almost appears to be polished and has a mirror-like appearance.

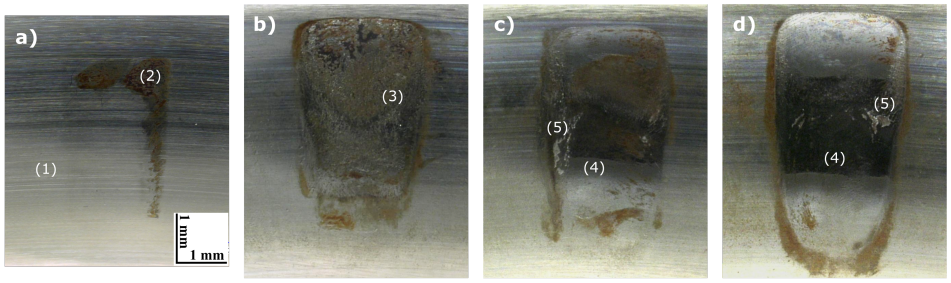

Figure 5. Damage on the inner Raceway of a 7208 rolling element bearing for different oscillation cycle numbers: (**a**) N = 1000, (**b**) N = 20,000, (**c**) N = 80,000, and (**d**) N = 160,000. Experimental parameters: contact pressure p_{max} = 2 GPa; oscillation angle $\theta = 7°$; oscillation frequency f = 5 Hz; grease: fully formulated Li grease; (1) indicates the undamaged raceway surface; (2) tribo-corrosion; (3) micropitts; (4) raceway surface with polished appearance; and (5) larger pittings.

The wear volumes of the individual wear marks are shown in Figure 6. For each bearing examined after a defined number of cycles, a corresponding polar plot is shown, divided into 14 segments and corresponding to the number of rolling elements. The mass loss of the marks on the inner ring is shown in green and the mass loss of the marks on the outer ring at the respective position on the bearing ring is shown in blue. The mass loss is determined by the measured wear volume and the density of 100Cr6 of $\rho_{100Cr6} = 7.8 \frac{g}{cm^3}$. After 1000 cycles, most of the marks are still undamaged and almost no macroscopic wear can be determined with the applied method. After 10,000 cycles, a clear increase in mass loss can be seen, especially on the outer ring. It is also clear that all marks around the circumference of the bearing show macroscopic wear, but the wear was not uniform across all the damage marks. While some marks already show a mass loss of 0.4 mg, other contact points lost less than 0.2 mg. The mass loss on the inner ring is still significantly lower than on the outer ring. After 20,000 cycles, a significant increase in mass loss can also be recorded on the inner ring. Here, the difference between the individual wear marks is even more noticeable. While individual marks show less than 0.1 mg, one wear mark already has a mass loss of 0.6 mg. As expected, the mass loss continues to increase with an increasing number of cycles and reaches its maximum at 160,000 cycles, which corresponds to the maximum number of tested cycles. Here, a maximum of approximately 1.2 mg per mark is measured on the inner ring.

Figure 7 shows the measured wear volumes in a box-plot. The wear volume is shown on the y axis and the number of cycles on the x axis. The determined values of the inner ring are again shown in green, and the values of the outer ring in blue. The median of the values is represented by a black dot in a white circle. The ends of the thick bars represent the 25 % quantile and 75 % quantile, respectively, the ends of the thin bars represent the minima and maxima, respectively, and the fetch circles represent the outliers in their corresponding color. It is noticeable that—as was to be expected from the previously shown figure—the scattering of the wear volumes per damage mark is large, i.e., not every rolling element raceway system behaves in the same way. If we follow the wear volume at the inner and outer ring, we notice a degressive trend with an increasing cycle number. A steep increase during the first 20,000 cycles was followed by a significantly shallower rise in the range of

80,000–160,000 cycles. It is also noticeable that the slope of wear volume on the outer ring is greater in the initial phase than the slope of the wear curve on the inner ring. Towards the end of the experiments, the slope equalizes.

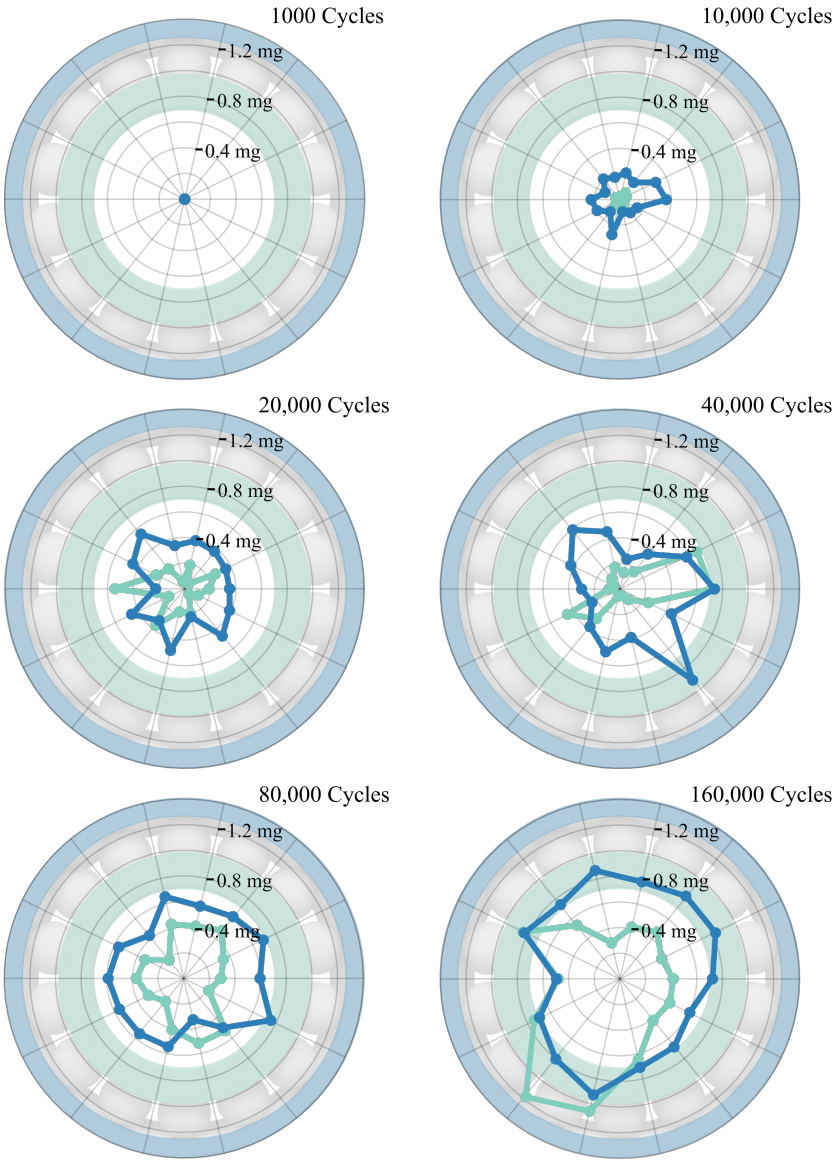

Figure 6. Representation of the mass loss of the individual damage marks on the raceway of the inner ring (green) and the raceway of the outer ring (blue) of the type 7208 bearings. The mass loss is calculated from the measured wear volume and the density $\rho_{100Cr6} = 7.8 \frac{g}{cm^3}$.

In order to establish a connection between the wear volume and torque, the progression of the maximum torque per oscillation cycle (black), the summed wear volume on the bearing raceway (blue), and the summed frictional energy are all shown versus the number of cycles in Figure 8. The course of the maximum torque starts at a low value of less than 2 Nm. After approximately 3000 cycles, the torque starts to increase steeply and reaches a local maximum value of approximately 23 Nm after approximately 50,000 cycles. Up to the end of the test at 160,000 cycles, the torque remains almost constant in the further course and only increases by approximately 1 Nm. The green curve in Figure 8 shows the accumulated dissipated energy, which results from the torque curves as described in Section 2.2. The frictional energy shows a degressive behavior, unlike what one would expect from the maximum torque. At this point, it is important to take a closer look at the

shape of the torque curves over the number of cycles. This is because, even if the maximum torque remains at an almost constantly high level towards the end of the test, the enclosed area within the torque curves decreases from a certain point in time onward.

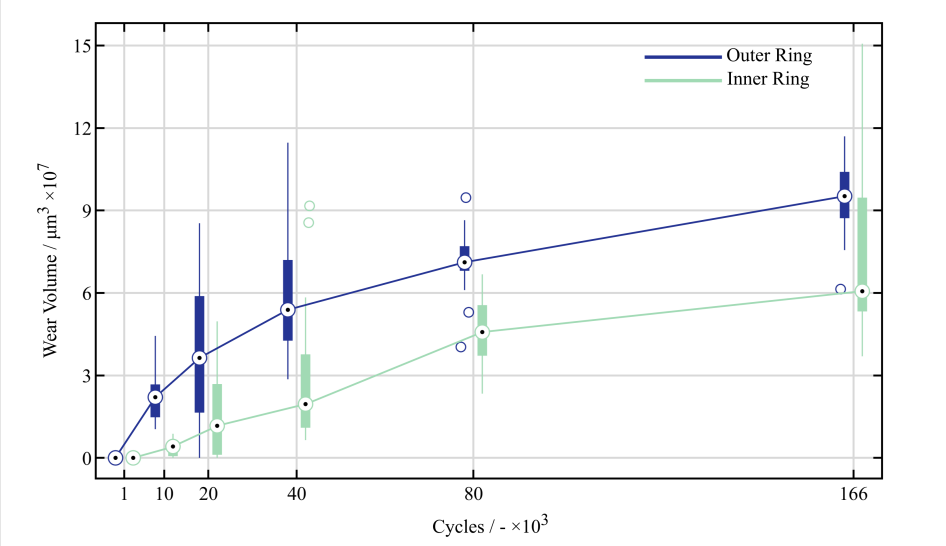

Figure 7. Box plot of the mass loss per contact area on the raceways of the type 7208 bearings against the number of oscillation cycles. The turquoise boxes represent the results for the inner raceway whilst the dark blue boxes represent the results for the outer raceway.

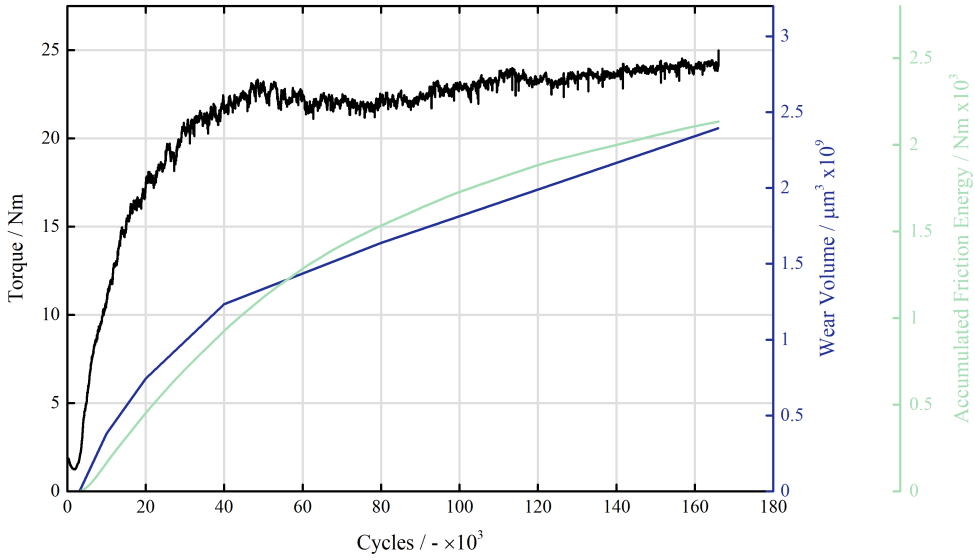

Figure 8. Courseof the maximum torque per oscillation cycle (black), the accumulated dissipated energy (green) and the linearly interpolated total wear volume (blue) over the number of cycles for the 7208 bearings.

Figure 9 shows selected torque curves at the times when the bearings were analyzed for wear. The torque curve after 1000 cycles, which is similar in shape to the curve one would expect for an undamaged bearing, is shown in light green, as can be seen in Section 2.2. After 10,000 cycles, the shape is still qualitatively similar to the expected curve for an undamaged bearing, but the torque during the oscillation cycle has already significantly increased. The maximum torque during the oscillation cycle of approximately 10 Nm is reached at approximately 1.5° after the reversal points. After 20,000 cycles, the shape of the curve starts to change. Peaks start to form at the reversal points, which are decisive for

the maximum torque in the following curves. However, even in the middle of the curve around an angle of 0°, the torque continued to increase. From this point on, pronounced peaks form at the reversal points, leading to an increase in the maximum torque. In the middle of the oscillation cycle, around an angle of 0°, however, the torque decreases. While values of ±8 Nm are observed at 0° for the curve at 20,000 cycles, after 160,000 cycles, only approximately ±2 Nm are measured.

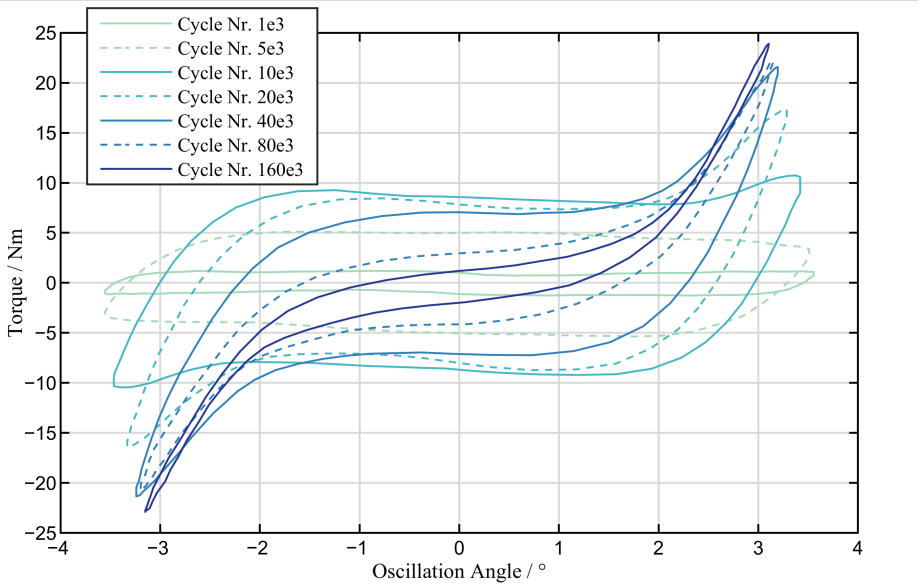

Figure 9. Plotof the torque curves versus the oscillation angle for selected oscillation cycles during the test with the type 7208 bearings.

The shown effects explain how the dissipated energy can be related to the maximum torque. In the last step, the relationship between the wear volume and dissipated energy is established. For this purpose, the linearly interpolated wear volume is divided by half of the accumulated dissipated energy at the current cycle number n to obtain an energy wear factor $\alpha_{v,n}$ according to FOUVRY.

$$\alpha_{v,n} = \frac{2 \cdot V_n}{\sum_{i=1}^{n} E_{d,i}} \tag{2}$$

This results in the energy wear factor $\alpha_{v,n}$ are shown in Figure 10. For the first 3000 cycles, which show no increase in torque, it is assumed that the grease lubrication is still effective in preventing wear in most contacts, so that $\alpha_{v,0-3,000} = 0$. From this point on, there is a steep increase to a value of approximately $99,171 \frac{\mu m^3}{J}$ at 10,000 cycles. Subsequently, $\alpha_{v,n}$ degressively decreases until becoming almost constant after 80,000 cycles. The horizontal black lines are energy wear coefficients measured by FOUVRY in a different test setup, which will be further discussed in Section 4.

3.2. Wear Development 7220

This paper aimed to identify the different wear mechanisms caused during the experiments by analyzing the torque signals during the tests and the the wear marks after the tests. In addition to the bearings of type 7208, this paper covers slightly larger bearings of type 7220. Despite the larger bearing size, the appearance of wear damage and its characteristics are very similar. Figure 11 shows a compilation of several photographic images of sections of wear marks produced with test parameters listed in Section 2.3.

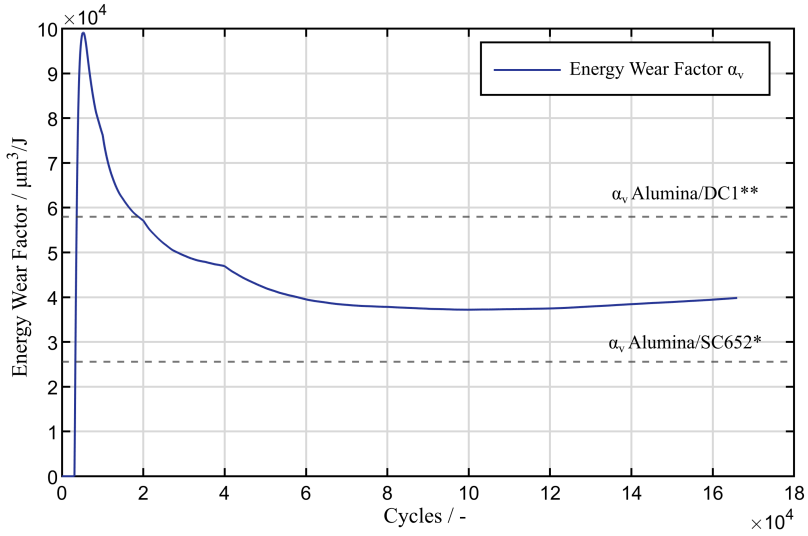

Figure 10. Representationof the energy wear factor determined here above the number of cycles (blue) for the type 7208 bearings. * Energy wear factor for an Alumina/SC652 contact in the oscillating ball–disk test under pure sliding found in [23]. ** Energy wear factor for an Alumina/DC1 contact in the oscillating ball-on-disc test with pure sliding found in [23].

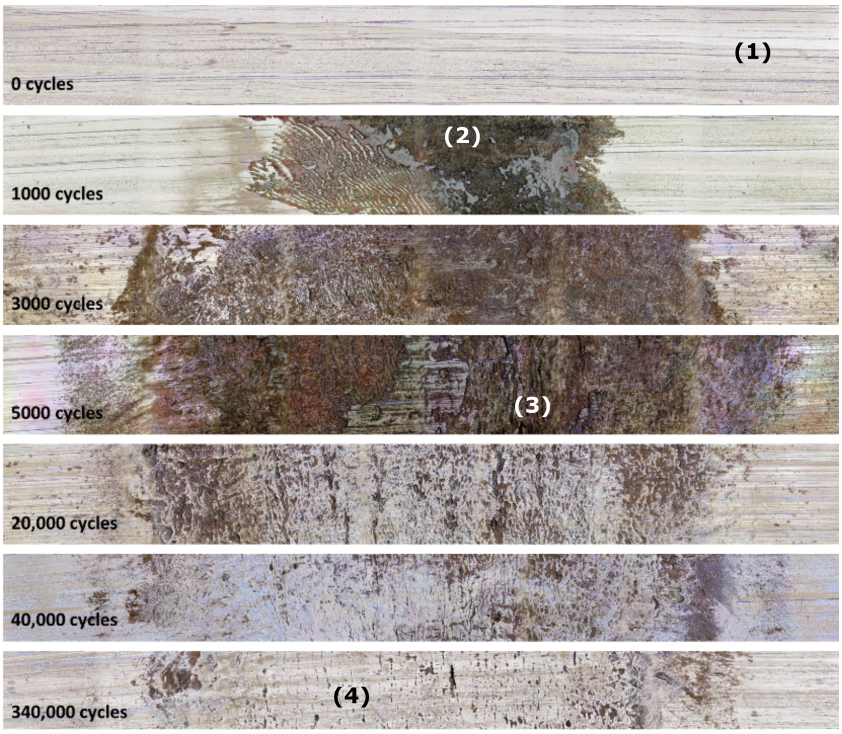

Figure 11. Sectional images of wear damage marks of type 7220 bearings for different oscillation numbers in ascending order (top–bottom): (1) undamaged raceway surface; (2) tribo-corrosion; (3) micropitts; and (4) raceway surface with polished appearance.

The phenomenological investigation of the wear marks shows different stages of wear damage. After approximately 1000 cycles, reddish-brown and blackish-brown corrosive products (tribo-corrosion) can be found on the raceway areas affected by the oscillating movements. With an increasing number of cycles, this corrosive wear spreads to almost the complete width of about $x + 2b$. In addition, the appearance of the surface becomes rougher and the local erosion of the surface is forming until 5000 cycles are reached. With a further increasing number of cycles, the damaged raceway appears more shiny and polished and

the corrosive products seem to disappear. However, there are no large differences between 40,000 and 340,000 cycles, despite the wear mark looking a bit more polished towards the center.

The optical analyses of the topography of the wear marks leads to the results described in this section. The differences in the different analysis methods applied with respect to the wear volume are described in Section 2.2.

Figure 12 shows the wear volume calculation of several investigated wear marks and tested bearings at different numbers of cycles. The data points are the mean values of several wear marks investigated with respect to the associated amount of cycles. The graph is characterized by a steep increase in the wear volume of between 500 and 40,000 oscillation cycles. Further increasing the number of cycles does not lead to a significant increase in wear volume. Even after 1 million cycles, the characteristic wear volume only roughly doubled compared to 40,000 cycles. However, the number of tests conducted for such a large amount of cycles is limited, which makes the interpretation somewhat difficult.

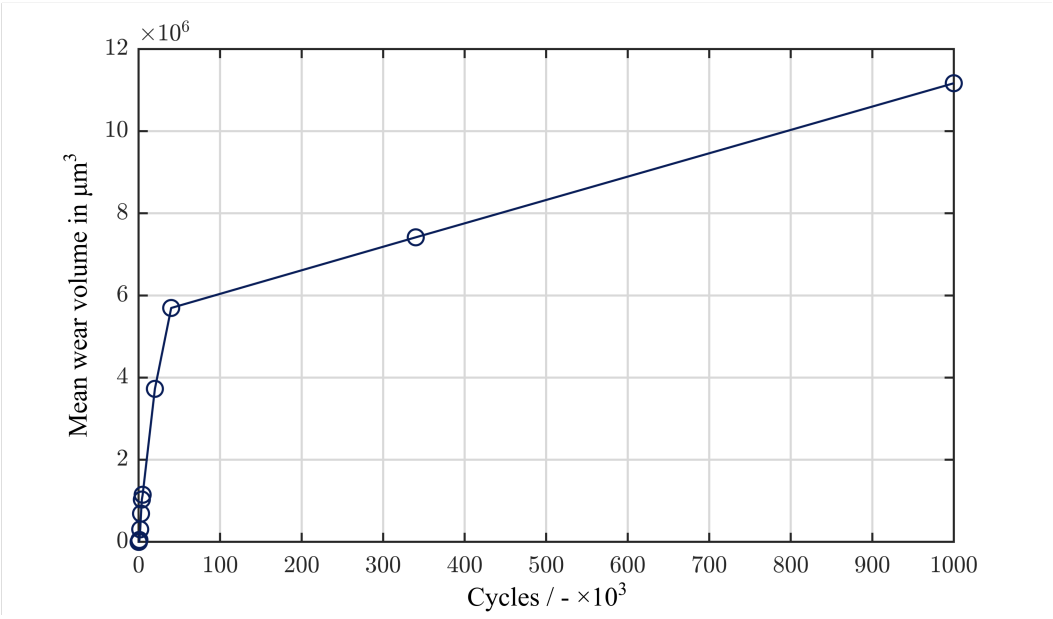

Figure 12. Meanvalue of wear volume per wear mark section for different numbers of oscillation cycles for the type 7220 bearings.

As discussed in the previous chapters, the torque signal is a strong indicator of wear damage forming on the raceways. Figure 13 shows the torque development for a test with 40,000 oscillation cycles and test parameters from Table 3.

The graph shows the peak torque value for each oscillation cycle during the test and the linearly interpolated wear volume from the data points in Figure 12 scaled according to Section 2.2 to represent one wear mark. The underlying test and its data will be investigated in more detail. The torque signal is characterized by a steep rise, starting with only a few cycles of movement. The steep rise has an almost linear characteristic starting from the load-dependent baseline torque of the bearings of approximately 15 Nm for the very first cycles and ending at approximately 55 Nm at approximately 10,000 cycles. Between 10,000 and 20,000 cycles, the torque level declines to approximately 35 Nm. No major change in the torque signal can be observed between 20,000 and 40,000 cycles. In contrast to the type 7208 bearings, the changes in the friction torque seem to happen at fewer oscillating cycles. Figure 14 shows the first 2000 oscillation cycles from Figure 13. The first 50 cycles are characterized by a decreasing friction torque. Afterwards, the friction torque increases according to the foregoing description.

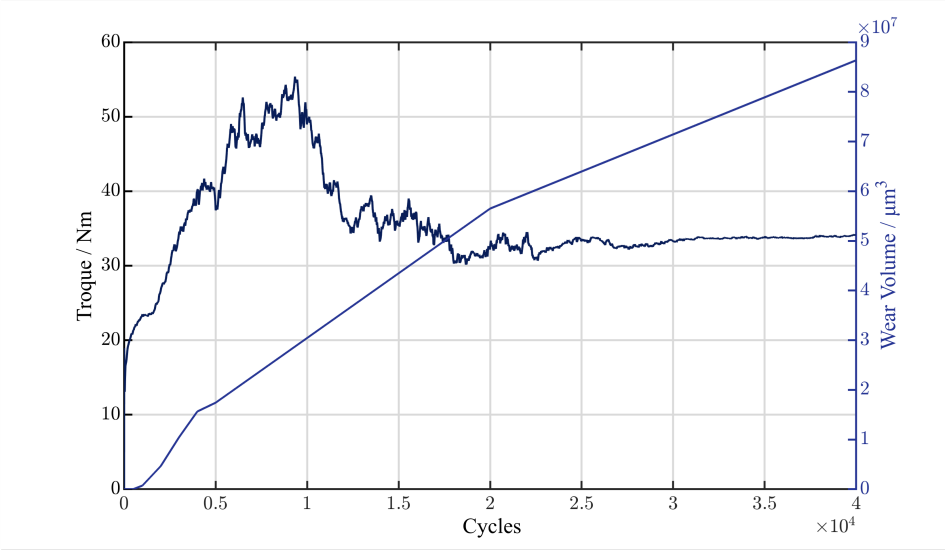

Figure 13. Peakof the torque signal as well as the interpolated and scaled wear volume of one wear mark for each oscillation cycle during a test with 40 k cycles on the type 7220 bearings.

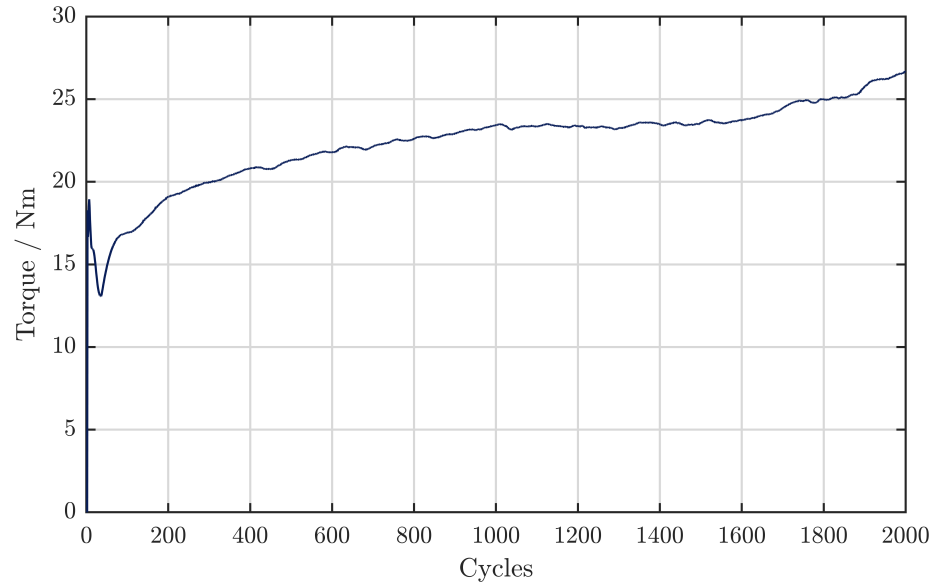

Figure 14. Peak of torque signal for the first 2000 cycles on the type 7220 bearings.

According to the phenomenological investigation of wear marks derived from tests with different numbers of cycles, different wear mechanisms seem to be present during the experiments distinguishable by the amount of oscillation cycles and the friction torque development. Besides analyzing the peak torque per cycle, the torque during an oscillation cycle reveals some changes throughout the experiments that point towards different wear mechanisms.

Figure 15 shows the torque signal plotted over the oscillation angle at different numbers of cycles during the same test as that in Figure 13. The oscillating movement with an oscillation angle of 4° was carried out at a mean oscillation angle of 0° with a sinusoidal characteristic. Hence, the turning points of the movements are at 2° and −2° and the 0° position is characterized by the highest rolling speed of approximately $6\,\frac{°}{s}$. Starting with the first cycles, the characteristic of the torque curve changes. Between 10 and 10,000 cycles, the torque signal rises noticeably at the 0° position where the speed is at its highest value. In addition, the torque level at the turning points also increases with more cycles leading to an overall larger area and the wider appearance of the torque curve. From 10,000 cycles

on, the shape of the torque curve changes its characteristics again. The torqu e level at high speeds seems to decrease, whereas the torque level at the turning points is increases even further.

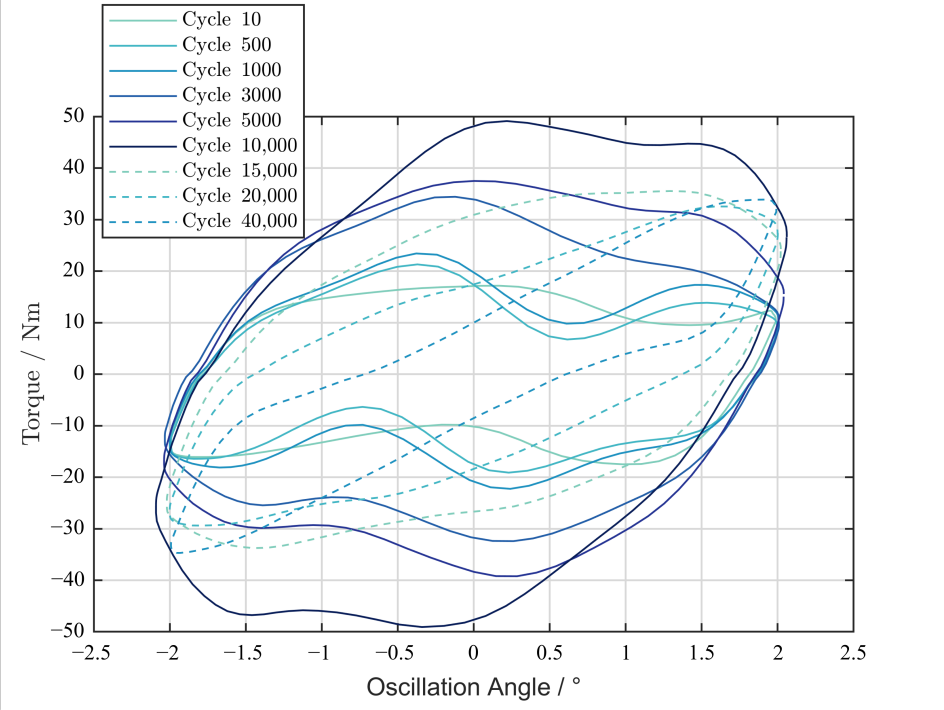

Figure 15. Torque curves versus oscillation angle plotted at different numbers of cycles during a test with a total of 40,000 cycles on the type 7220 bearings.

A similar behaviour can be observed in Figure 9 during the tests with type 7208 bearings. As indicated in the previous chapter, the change in shape of the torque curves is associated with a degressive change in dissipated energy during every cycle. Analogous to the analysis of the smaller bearings, the relationship between the wear volume and dissipated energy is evaluated for the type 7220 bearings. Hence, the energy wear factor according to (2) is calculated for the underlying test. Characterized by the friction torque development over the first cycles, no wear damage is considered for the first 50 cycles due to the slight decrease in friction torque. However, the steep increase in friction torque for the continuing cycles is associated with failing lubrication but wear volume measurements and the images of wear mark show (as can be seen in Figure 11) that it takes approximately 1000 cycles to form the first corrosive wear damages and loss of material. Figure 16 shows the calculated energy wear factor for the underlying test of type 7220 bearings with 40,000 cycles. Similarly to the smaller bearings, it is characterized by a steep increase over the very first cycles, beginning at approximately 500 cycles. However, the peak value is reached earlier than for the 7208 bearings. The energy wear factor decreases after the peak value and reaches an almost constant value of approximately $46,000\ \frac{\mu m^3}{J}$ at 10,000 cycles.

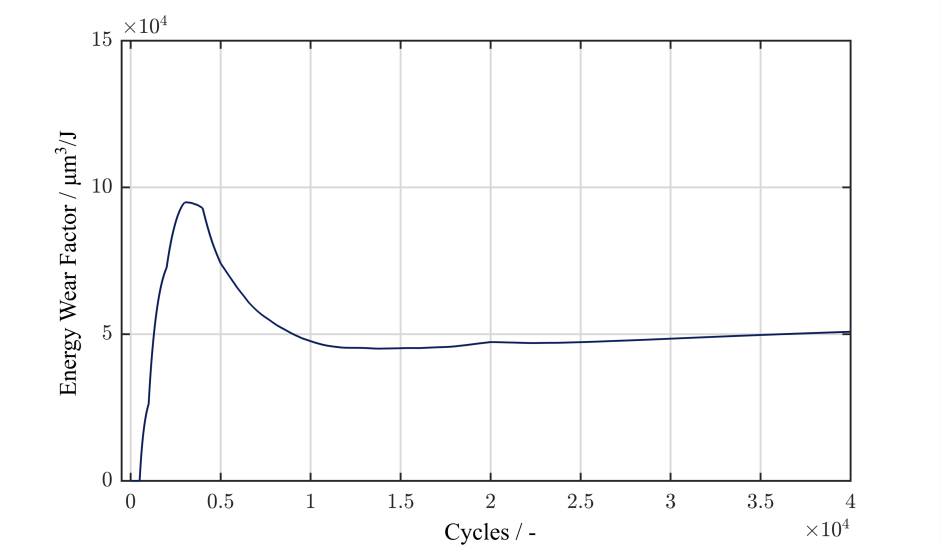

Figure 16. Energywear factor for a test with type 7220 bearings and 40,000 cycles according to Section 2.3.

4. Discussion

Parameter studies (see [6,18]) have shown that, under certain operating conditions, it is possible for grease-lubricated oscillating rolling bearings to operate without damage, at least in the short term. However, if the operating conditions result in severe starvation and solid contact between the rolling element and raceway, adhesion between the contact partners can occur due to the similarity in the materials. If micro-welds are torn apart by a forced movement, material pitting and particle formation will occur. The resulting particles have a high specific and reactive metallic surface area, which leads to the oxidation of these particles. In the initial phase of the experiments shown, roughened surfaces with small material spalls as well as color changes indicative of corrosion can be seen in the damage marks. This is accompanied by a significant increase in torque over the entire oscillation cycle and a high energy wear coefficient. Based on these observations, the authors assume that the primary damage mechanism adhesion is responsible for the false brinelling damage in the initial phase, as was also assumed by TOMLINSON, GODFREY, and ALMEN. In the further course of wear process, the wear ground of the damage marks is increasingly smoothed.

The reason for the smoothing could be oxide particles, which act as an abrasive third body in the rolling element raceway contact due to their high hardness and chemical inertness. The particles are ground into increasingly finer particles in contact and act as a separating abrasive intermediate medium that prevents direct metallic contact and thus adhesion between the rolling element and raceway. For the raceway surface, the particles, which may be mixed with lubricant to form a paste, act as abrasive polish and lead to smoothing and the mirror-like appearance of the wear base. The hypothesis that an abrasive mechanism is dominant in the later stages of the test is supported by the fact that the energy-wear factor $\alpha_{v,n}$ has a comparable magnitude to the factors determined by FOUVRY [23]. Here, FOUVRY investigated material pairings, which are not prone to adhesion due to their material properties, but to abrasive and corrosive wear. In Figure 10, two lines with constant energy wear coefficients are plotted, which were determined in their pin-on-disc experiments. The lower line at 25,600 $\frac{\mu m^3}{J}$ was determined for a material pairing of alumina and HSS-Steal, whilst the upper line at approximately 57,000 $\frac{\mu m^3}{J}$ was determined for a pairing of and alumina and sintered steel (DC1). The material properties, including those of 100Cr6, of which the bearings and rolling elements investigated herein are made, are listed in Table 4. It should be noted that FOUVRY'S tests were performed on dry contacts without lubrication. Since the energy-wear coefficients are nevertheless of a similar order

of magnitude to the bearing tests under grease lubrication, it can be assumed that the lubricant only initially has a wear-inhibiting effect, but becomes almost useless in the course of the tests. This paper shows the results from tests conducted with two different bearing sizes lubricated with the same grease. All foregoing descriptions of the different wear mechanisms applied to both bearing sizes. However, there are differences in the test results. Looking at Figure 17, the wear initiation and the transition between the adhesion and abrasion occurred earlier for the larger bearings.

For the investigations, it was assumed that the lubrication is effective until a torque increase can be recorded. Up to this torque increase, it is assumed in a simplified way that the dissipated energy mainly results from the shearing of the fluid in the contact and does not have a relevant share in the raceway wear. From the torque increase onward, it is assumed that a parched contact is present and that the dissipated energy can be directly related to the occurring wear. Figure 17 shows the two curves of the energy wear factor α_v for the two bearing types 7208 (blue) and 7220 (green). It is noticeable that the blue curve only starts to increase at approximately 3000 cycles, whereas the green curve already starts to increase after 50 cycles. The maximum of the two curves is shifted by approximately the same cycle amount. The transition from the adhesive damage range with an increased energy wear factor to the abrasive damage range with an almost constant lower-energy wear factor occurs earlier and is somewhat steeper in the larger bearings (green) than in the small bearings (blue). The reason for the fact that the damage process starts earlier and proceeds faster in the larger bearings is possibly the lubricant behavior close to the contact. The long semi-axis a of the contact ellipse for the tests of the 7220 bearings is approximately twice as long as for the 7208 bearings. If one assumes that, after an initial phase in which the grease is displaced from the contact by the oscillating motion, the base oil bleeding from the side reservoirs has a decisive influence on the lubrication of the contact. A larger half-axis a of the contact is disadvantageous as shown by the investigations of CEN into the starved lubrication of rotating grease lubricated bearings [29]. BEHNKE ET AL. also showed results of the wear tests of real-size blade bearings with the same grease as the lubricant [5]. For the smaller amplitude ratios, the wear already occurred for only 1000 cycles, which matches the fast wear initiation obtained in the tests with the type 7220 bearings in this paper. Another reason for the shorter initial damage-free phase in the type 7220 bearings may also be the higher contact pressure of 2.5 GPa compared to 2 GPa in the type 7208 bearings. The higher pressure may be conducive to grease displacement from the rolling contact. Furthermore, the running-in process of the bearings in which a redistribution of the grease reservoirs takes place is longer in the tests with the 7220 bearings than with the 7208 bearings. In the case of the 7220 bearings, approximately 100 revolutions of continuous rotation were carried out before the start of the test, while in the case of the 7208 bearings, there were only 20 rotations. The redistribution of grease during rotation could cause the grease reservoirs close to the contact to become smaller over time and provide a poorer base oil supply to the contact in the subsequent oscillatory motion.

A further open question is that of the extent to which the damage shown is relevant for the operation of the bearings in the application. In applications where the drive power of the motors is limited, e.g., in space applications, even a small increase in the bearing torque can cause the drive to block completely [30–32]. In this case, the initiation of false brinelling damage must be prevented at all costs. In applications where the bearings are only temporarily subjected to oscillations and are subsequently operated under continuous rotation, the resulting wear marks on the surface can lead to significant noise generation [8,33]. In addition, rolling over the edges of the wear marks that evolve under oscillating conditions can lead to an increase in surface and subsurface stresses, which in turn promote material fatigue and can lead to a reduction in service life [34]. For the operation of a rotor blade bearing, minor wear damage in the initial phase is not a problem, since the blade pitch mechanisms provide sufficient torque to overcome it. However, it has not yet been sufficiently researched how this false brinelling damage affects

secondary damage such as raceway fatigue. If the material loss in the raceway subsequently becomes excessive, jamming and consequential damage to the bearing cage can occur [35].

Minor pittings were observed in the damage marks, contributing to the wear progress. However, significant crack propagation into the interior of the material, as observed in standstill marks under amplitude ratios of $x/2b < 1$ ([9,11]), is not to be expected under the conditions at amplitude ratios of $x/2b > 1$ [9]. Whether and from when classical subsurface initiated rolling fatigue plays a role in the damage marks in the later course is not yet known. The deepest damage marks of the 7208 bearings on the inner ring had a depth of approximately 60 µm after 160,000 oscillation cycles. A simple estimation of the depth of the maximum orthogonal shear stress, neglecting the near-surface excess stresses, leads to a depth of $z_0 = 0.5 \cdot b = 650\,\mu m$ [36]. A simple estimate of the L_{10} life leads to $L_{10} = \left(\frac{C_1}{P_1}\right)^p = 125 \cdot 10^6$ revolutions [37]. Per revolution, a volume element on the inner ring is rolled over approximately 8 times in the 7208 bearings. At $125 \cdot 10^6$ revolutions, this is approximately $N_{rot} = 10^9$ rollovers. At 160,000 oscillation cycles, the loaded volume elements are rolled over about $N_{osc} = 320,000$ times. This leads to a factor of $\frac{N_{rot}}{N_{osc}} = 3125$. The ratio of the depth of maximum orthogonal shear stress z_0 and the maximum reached wear depth on the inner ring after 320,000 rollovers z_{ir} is $\frac{z_0}{z_{ir}} \approxeq 11$. As such, it is conceivable that the wear rate is so high that classical rolling fatigue does not matter. Of course, this is only a very simple rough calculation to obtain a feeling for the order of magnitude of the investigated cycle numbers, which does not take into account the reduced loaded volume due to oscillation, nor the change in topography and the associated change in stresses. Furthermore, the change in microstructure at the worn surface and its influence on crack initiation and propagation is not considered here [38].

Table 4. Material properties; properties of alumina, HSS, and DC1 are taken from FOUVRY [23], properties of 100Cr6 are taken from [39].

	Young's Modulus, E (GPa)	**Poisson Coefficient, ν**	**Hardness, H (HV)**
100Cr6	210	0.3	800
Alumina (Counterbody)	370	0.27	2300
HSS (SC652)	230	0.28	800
DC1 (Sintered Steel)	200	0.3	370

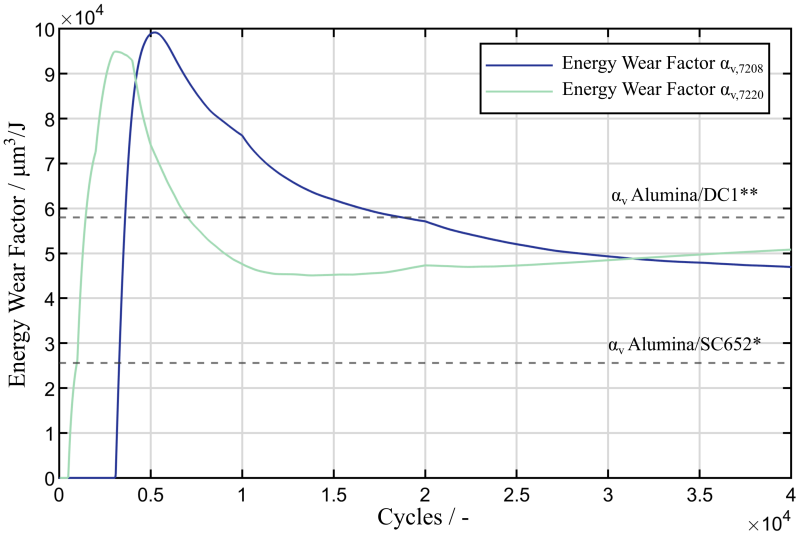

Figure 17. Comparisonof the curves of the energy wear factors for the tests with bearing type 7208 (green) and 7220 (blue). * Energy wear factor for an Alumina/SC652 contact in the oscillating ball–disk test under pure sliding found in [23]. ** Energy wear factor for an Alumina/DC1 contact in the oscillating ball-on-disc test with pure sliding found in [23].

To be on the safe side, protective mechanisms such as lubrication cycles as proposed by STAMMLER ET AL. should therefore take place before a sharp increase in bearing torque due to lubrication failure and the onset of adhesive and corrosive damage. However, it has not yet been sufficiently clarified how exactly such damage affects the service life of, for example, a rotor blade bearing.

5. Conclusions

The results shown in this paper have illustrated the development of false brinelling damage both in terms of the visual appearance of the damage on the raceway and the volume of wear on the raceway. The results obtained from the experiments carried on the angular contact ball bearings of different sizes (type 7208, type 7220) show that false brinelling damage starts from adhesion and corrosion after an initial incubation period during which the lubricant can prevent severe damage on the raceway. This damage is manifested by red and black-brown discoloration and material pitts on the raceway surface. Damage initiation is accompanied by a steep increase in torque and wear volume. Damage initiation occurs earlier with larger bearings, presumably due to the poorer lubricant supply to the contact because of the larger contact ellipse. The energy wear factor, which indicates how much wear volume occurs per dissipated energy, shows a maximum in the initial phase, after approximately 3000 cycles for the type 7220 bearings and after approximately 5000 cycles for the type 7208 bearings. In this range, it is assumed that the adhesive and corrosive damage mechanisms predominate. As the number of cycles increases, the energy wear factor decreases to approximately half of its maximum for both bearing types and remains at a near constant level from 10,000 cycles for the type 7220 bearings and from approximately 40,000 cycles for the type 7208 bearings onward. In this phase, the visual appearance of the marks changes from red or black-brown discoloration with pits to increasingly smooth mirror-like appearing wear marks with increasing depth. Based on this appearance, it is assumed that an abrasive damage mechanism predominates in this phase. This assumption is consistent with the observation that the energy wear factor in this phase is approximately as large as the energy wear factors measured by FOUVRY for abrasive wear in a ball-on-disc contact [23]. It must be noted, however, that these are experimental conditions that are fundamentally different and a quantitative comparison only serves as a rough guide. Finally, it can be concluded from the results that even a small number of cycles can lead to severe wear on the raceway surface. The initial phase is particularly critical due to the adhesive and corrosive wear mechanisms present. In addition, the initiation of wear seems to start significantly earlier in the larger rolling contact, which appears to be particularly critical with regard to the use in full-size rotor blade bearings.

Author Contributions: Conceptualization, S.W. and A.B.; methodology, S.W. and A.B.; validation, S.W. and A.B.; formal analysis, S.W., A.B. and J.G.; investigation, S.W., A.B. and N.B.; resources, S.W., A.B. and G.P.; writing—original draft preparation, S.W. and A.B.; writing—review and editing, S.W., A.B., N.B. and G.P.; visualization, S.W., A.B. and J.G.; supervision, G.P.; project administration, S.W., A.B. and G.P.; funding acquisition, S.W., A.B. and G.P. All authors have read and agreed to the published version of the manuscript.

Funding: This document is a result of the research projects "iBAC—Intelligent Blade Bearing Amplitude Control" (grant number: 0324344A) and "HBDV—Highly Loaded Slewing Bearings" (grant number: 0324303A) funded by the Federal Ministry for Economic Affairs and Climate Action (Federal Republic of Germany) and of the project.

Data Availability Statement: The data presented in this study are available on request from the corresponding author.

Acknowledgments: The authors would like to thank Bela Lehnhardt for their support in assembling the bearings for the experiments.

Conflicts of Interest: The authors declare no conflicts of interest. The funders had no role in the design of the study; in the collection, analyses, or interpretation of data; in the writing of the manuscript; or in the decision to publish the results.

Abbreviations

The following abbreviations are used in this manuscript:

ACBB	Angular Contact Ball Bearing
HSS	High-Speed Steel
IPC	Individual Pitch Control
CPC	Collective Pitch Control
Z	Number of Rolling Elements
C_1	Basic Dynamic Load Rating
P_1	Equivalent Dynamic Bearing Load
L_{10}	Basic Fatigue Life Rating
f	Oscillation Frequency
θ	Oscillation Angle
$x/2b$	Amplitude Ratio/Ratio of Moved Distance x to Double Half-Width of the Contact Ellipse b
p_{max}	Maximum Contact Pressure
d_o	Outer Diameter
T_s	Steady State Torque
T_{max}	Maximum Torque
E_d	Dissipated Friction Energy
α_v	Energy Wear Factor

References

1. Burton, T. *Wind Energy Handbook*, 2nd ed.; John Wiley & Sons: Hoboken, New Jersey, USA, 2011.
2. Bossanyi, E.A. Individual blade pitch control for load reduction. *Wind Energy Int. J. Prog. Appl. Wind Power Convers. Technol.* **2003**, *6*, 119–128. [CrossRef]
3. Barlas, T.K. Review of state of the art in smart rotor control research for wind turbines. *Prog. Aerosp. Sci.* **2010**, *46*, 1–27. [CrossRef]
4. Stammler, M.; Thomas, P.; Reuter, A.; Schwack, F.; Poll, G. Effect of load reduction mechanisms on loads and blade bearing movements of wind turbines. *Wind Energy* **2020**, *23*, 274–290. [CrossRef]
5. Behnke, K.; Schleich, F. Exploring Limiting Factors of Wear in Pitch Bearings of Wind Turbines with Real Scale Tests. *Wind Energy Sci. Discuss.* **2022**, *2022*, 1–22. [CrossRef]
6. Wandel, S.; Bader, N.; Schwack, F.; Glodowski, J.; Lehnhardt, B.; Poll, G. Starvation and relubrication mechanisms in grease lubricated oscillating bearings. *Tribol. Int.* **2022**, *165*, 107276. [CrossRef]
7. Schwack, F.; Halmos, F.; Stammler, M.; Poll, G.; Glavatskih, S. Wear in wind turbine pitch bearings—A comparative design study. *Wind Energy* **2022**, *25*, 700–718. [CrossRef]
8. Almen, J.O. Lubricants and False Brinelling of Ball and Roller Bearing. *J. Mech. Eng.* **1937**, *59*, 415–422.
9. Vingsbo, O.; Söderberg, S. On Fretting Maps. *Wear* **1988**, *1988*, 131–147. [CrossRef]
10. Grebe, M.; Molter, J.; Schwack, F.; Poll, G. Damage mechanisms in pivoting rolling bearings and their differentiation and simulation. *Bear. World J.* **2018**, *3*, 72–85.
11. Grebe, M. False Brinelling—Standstill Marks at Roller Bearings. Ph.D. Thesis, Slovak University of Technology, Bratislava, Slovakia, 2012.
12. Schwack, F. Untersuchungen zum Betriebsverhalten Oszillierender Wälzlager am Beispiel von Rotorblattlagern in Windenergieanlagen. Ph.D. Thesis, Leibniz Universität Hannover, Hannover, Germany, 2020.
13. Schadow, C. Stillstehende Fettgeschmierte Wälzlager unter Dynamischer Beanspruchung. Ph.D. Thesis, Otto-von-Guericke-Universität, Magdeburg, Germany, 2016.
14. Kita, T.; Yamamoto, Y. Fretting wear performance of lithium 12-hydroxystearate greases for thrust ball bearing in reciprocation motion. *Jpn. J. Tribol.* **1997**, *42*, 782–783.
15. Shima, M.; Jibiki, T. Fretting wear. *J. Jpn. Soc. Tribol.* **2008**, *53*, 462–468.
16. Maruyama, T.; Saitou, T.; Yokouchi, A. Differences in Mechanisms for Fretting Wear Reduction between Oil and Grease Lubrication. *Tribol. Trans.* **2016**, *60*, 497–505. [CrossRef]
17. Saatchi, A. The Effect of Grease Composition on Fretting Wear. Ph.D. Thesis, University of Akron, Akron, OH, USA, 2019.
18. Wandel, S.; Bader, N.; Glodowski, J.; Lehnhardt, B.; Leckner, J.; Schwack, F.; Poll, G. Starvation and Re-lubrication in Oscillating Bearings: Influence of Grease Parameters. *Tribol. Lett.* **2022**, *70*, 1–14. [CrossRef]

19. *ASTM D4170*; Standard Test Method for Fretting Wear Protection by Lubricating Greases. American Society for Testing and Materials: Conshohocken, PA, USA, 2016.
20. *NFT 60-199*; Aptitude à résister au faux Effet Brinell. Association française de normalisation: Saint-Denis, France, 1995.
21. Stammler, M. Endurance Test Strategies for Pitch Bearings of Wind Turbines. Ph.D. Thesis, Fraunhofer Verlag: Stuttgart, Germany, 2020.
22. Stammler, M.; Poll, G.; Reuter, A. The influence of oscillation sequences on rolling bearing wear. *Bear World J.* **2019**, *4*, 19–25.
23. Fouvry, S.; Liskiewicz, T.; Kapsa, P.; Hannel, S.; Sauger, E. An energy description of wear mechanisms and its applications to oscillating sliding contacts. *Wear* **2003**, *255*, 287–298. [CrossRef]
24. Dahl, P. *A Solid Friction Model*; Technical report; Aerospace Corp: El Segundo Ca, CA, USA, 1968.
25. Todd, M.; Johnson, K. A model for coulomb torque hysteresis in ball bearings. *Int. J. Mech. Sci.* **1987**, *29*, 339–354. [CrossRef]
26. Godfrey, D. *Investigation of Fretting Corrosion by Microscopic Observation*; Technical Report 2039; National Advisory Committee for Aeronautics: Cleveland, OH, USA, 1950.
27. Tomlinson, G.; Thorpe, P.; Gough, H. An investigation of the fretting corrosion of closely fitting surfaces. *Proc. Inst. Mech. Eng.* **1939**, *141*, 223–249. [CrossRef]
28. Sakmann, B.; Rightmire, B. *An Investigation of Fretting Corrosion under Several Conditions of Oxidation*; Technical Report 1492; NASA: Washington, DC, USA, 1948.
29. Cen, H.; Lugt, P.M. Replenishment of the EHL contacts in a grease lubricated ball bearing. *Tribol. Int.* **2020**, *146*, 106064. [CrossRef]
30. Bohner, J.J.; Conley, P.L. On the torque and wear behavior of selected thin film MOS2 lubricated gimbal bearings. In *Proceedings of the 22nd Aerospace Mechanisms Symposium*; Langley Research Center: Hampton, VA, USA, 1988; pp. 227–244
31. Phinney, D.D.; Pollard, C.L.; Hinricks, J.T. Experience with duplex bearings in narrow angle oscillating applications. In *Proceedings of the 22nd Aerospace Mechanisms Symposium*; Langley Research Center: Hampton, VA, USA, 1988; pp. 211–216.
32. Loewenthal, S.H. Two Gimbal Bearing Case Studies: Lessons Learned. In *Proceedings of the 22nd Aerospace Mechanisms Symposium*; Langley Research Center: Hampton, VA, USA, 1988; pp. 253–269.
33. Godfrey, D. Fretting corrosion or false brinelling? *Tribol. Lubr. Technol.* **2003**, *59*, 28–31.
34. Schadow, C.; Deters, L. *Abschlussbericht Forschungsvorhaben Nr. 540 I: False Brinelling—Stillstehende fettgeschmierte Wälzlager unter dynamischer Belastung*; Technical Report 951; Forschungsvereinigung Antriebstechnik e.V.: Frankfurt am Main, Germany, 2010.
35. Buescher, M.; Leupold, S.; Schelenz, R.; Jacobs, G. Cage Loads of Wind Turbine Blade Bearing. In *Proceedings of the Journal of Physics: Conference Series*; IOP Publishing: Bristol, UK, 2020; Volume 1618, p. 052061.
36. Brändlein, J. *Die Wälzlagerpraxis. Handbuch für die Berechnung und Gestaltung von Lagerungen*, 3rd ed.;Vereinigte Fachverlage: Mainz, Germany, 1995.
37. Harris, T.A.; Kotzalas, M.N. *Rolling Bearing Analysis—Essential Concepts of Bearing Technology*, 5th ed.; Taylor & Francis: London, UK, 2007.
38. Yan, H.; Wei, P.; Su, L.; Liu, H.; Wei, D.; Zhang, X.; Deng, G. Rolling-sliding contact fatigue failure and associated evolutions of microstructure, crystallographic orientation and residual stress of AISI 9310 gear steel. *Int. J. Fatigue* **2023**, *170*, 107511. [CrossRef]
39. Bhadeshia, H. Steels for bearings. *Prog. Mater. Sci.* **2012**, *57*, 268–435.